RSC Advances

PAPER

View Article Online
View Journal | View Issue

Cite this: *RSC Adv.*, 2020, **10**, 33608

Treatment of *Staphylococcus aureus* skin infection *in vivo* using rifampicin loaded lipid nanoparticles

Anna Walduck,[a] Parveen Sangwan,[b] Quynh Anh Vo,[bc] Julian Ratcliffe,[b] Jacinta White,[b] Benjamin W. Muir *[b] and Nhiem Tran*[a]

Received 14th July 2020
Accepted 2nd September 2020

DOI: 10.1039/d0ra06120d

rsc.li/rsc-advances

We have previously reported on a novel nanoparticle formulation that was effective at killing *Staphylococcus aureus in vitro*. Here, we report for the first time, the antibacterial effects of a lipidic nano-carrier containing rifampicin (**NanoRIF**) which can be used to successfully treat Methicillin-Resistant *S. aureus* (MRSA) infection at a reduced antibiotic dosage compared to the free drug in a skin wound model in mice. The formulation used contains the lipid monoolein, a cationic lipid *N*-[1-(2,3-dioleoyloxy)propyl]-*N*,*N*,*N*-trimethylammonium methyl-sulfate (**DOTAP**) and the antibiotic. We have shown that rifampicin-loaded nanoparticles are more effective at treating infection in the skin wound model than the antibiotic alone. Cryo-TEM was used to capture for the first time, interactions of the formed nanoparticles with the cell wall of an individual bacterium. Our data strongly indicate enhanced binding of these charged nanoparticles with the negatively charged bacterial membrane. The efficacy we have now observed *in vivo* is of significant importance for the continued development of nanomedicine-based strategies to combat antibiotic resistant bacterial skin infections.

1. Introduction

Developing new delivery vehicles and compounds to aid in the treatment of antibiotic resistant bacterial infections is a global public health challenge of growing urgency.[1] The misuse of antibiotics has resulted in the emergence of Multi-Drug Resistant (MDR) bacteria.[2] It is becoming increasingly common for bacteria to gain MDR across different classes of antibiotics.[3–7] Therefore, it is important that the research community contribute to the development of more effective therapies to treat MDR bacterial infections, including Methicillin-Resistant *Staphylococcus aureus* (MRSA),[8] a common cause of skin and other infections, which can be fatal.[9–15]

The use of nanoparticles that encapsulate antibiotics shows great promise, potentially improving the efficacy of currently available compounds whilst reducing the risk of overuse leading to MDR bacteria.[16–21] The advantages of these nanoparticles include the fact that they may preferentially accumulate at infected sites due to poorly built neovasculature in diseased tissues which is commonly referred to as the enhanced permeability and retention (EPR) effect.[22,23] The EPR effect was first observed in solid tumours where macromolecules and nanoparticles tend to accumulate in large quantities due to their increased vascular permeability and reduced lymphatic drainage. This discovery has resulted in a paradigm shift in anti-cancer drug design, including a strong rationale for using nanoparticle-based delivery vehicles. Several studies have shown that the EPR effect is not limited to solid tumours and has been observed in bacterial infections'.[3,24–26] Azzopardi *et al.* provide an excellent review summarising the enhanced permeability and retention effect for drug targeting infection.[23] There are a number of possible shared pathophysiological pathways in infection and cancer and a new class of novel nanomedicines which have been termed 'Nanoantibiotics',[27] are showing promise in passive accumulation at infected sites *in vivo*.[18] Sikkink *et al.* have shown enhanced uptake of radiolabelled PEG-coated liposomes in intra-abdominal abscesses which could be rationalised by the presence of an EPR effect from the infection and selective accumulation of the nanoparticles at the site of infection.[28] Similar to the hypervasculature found in solid tumours, inflammation and infection may be associated with angiogenesis and high vascular density.[29] The nanoparticles are believed to be retained at the infected site by phagocytic cells such as macrophages.[30] The similarity between cancer and infection may also be a dysfunctional lymphatic system, an essential characteristic of the EPR phenomenon in cancer. It has been proposed that increased interstitial pressure and tissue destruction due to infection may be causes for reduced lymphatic drainage.[31] Following on from an initial infection, vasodilation rapidly occurs which results in wound site swelling and angiogenesis which may aid in the retention of macromolecules and

[a]*School of Science, RMIT University, 124 La Trobe Street, Melbourne 3000, Victoria, Australia. E-mail: nhiem.tran@rmit.edu.au*

[b]*CSIRO Manufacturing, Bag 10, Clayton South 3169, Victoria, Australia. E-mail: ben.muir@csiro.au*

[c]*Chimie Paris Tech, Paris, France*

nanoparticles at wound sites. The EPR effect has also been shown to reduce side effects and enable greater concentrations of antibiotics to be administered to infected patients. Other benefits with the use of nanoparticles include their ability to be designed to enhance their interaction with bacterial cell walls through various protein and antibody-ligand bindings or *via* electrostatic forces.[3,32,33]

A particularly interesting class of potential antibiotic nanocarriers is based on self-assembled lyotropic liquid crystalline lipid materials which display unique internal nanostructures.[34,35] Under physiological conditions, the bulk lipid can form nano-porous mesophase structures including lamellar, inverse bicontinuous cubic, hexagonal, and sponge phases.[33,36] The lipid used in this study (monoolein) is a lyotropic liquid crystal forming bulk lipid. The mesophases (lamellar, cubic, hexagonal, sponge) are normally referred to as the structure which arises from the bulk lipid which is used to form them. When the bulk lipid is dispersed into nanoparticles, they form colloids (liposomes, cubosomes, hexosomes, and nano sponges). The lipid nanoparticles in this study are defined as lyotropic liquid crystalline nanoparticles which are colloidally and thermodynamically stable nanoparticles. The lipid bilayers of a bicontinuous cubic phase for example, can be described by a mathematical structure of infinite periodic minimal surfaces (IPMS), which have zero mean curvature. The mesophase structure of bicontinuous cubic phases have been reviewed previously together with other mesophases formed by lyotropic liquid crystalline materials.[37,38] In terms of the production and characterisation of mesophase nanoparticles, Demurtas *et al.* performed a very interesting study using tomographic-cryo-TEM to elucidate the structure of bicontinuous cubic phases in cubosomes.[39] After the creation of a colloidally stable dispersion through the use of a stabiliser, nanoparticles of liposomes, cubosomes, hexosomes, and nano sponges can be produced. The commonly used pluronic stabiliser, F127, is amphiphilic and interacts with the lipid bilayer to provide colloidal stabilisation to the cubosomes used in this work. As these nanomaterials are amphiphilic they can be used to encapsulate both hydrophilic and hydrophobic compounds.[40,41]

Nanomedicine based formulations utilising liposomes are most commonly used in cancer therapies.[42–45] It has been shown however that for some applications the use of cubosomes, hexosomes and nano sponges with more complex internal nanostructures may be advantageous.[34,40,41,46–48] The significantly larger interfacial surface areas in these mesophases can enable a greater concentration of drug molecules to be incorporated and the release rates may also be modulated.[49,50] Through the bioconjugation of targeting proteins, cubosomes for example, have been shown to be more effective than liposomes in some applications.[48] Due to these potential benefits a number of non-lamellar self-assembled lipid nanoparticles are currently under investigation as drug delivery platforms for various compounds including cancer drugs, antimicrobial peptides and proteins.[51–57]

In this study, we have used our previously optimised and reported non-lamellar lipid nanoparticles formed with monoolein (**MO**) and stabilised with Pluronic F127 as the bulk carrier.[52] **MO** is a biocompatible lipid, extensively studied for use in drug delivery applications. Positively charged lipid nanoparticles (**NanoRIF**), which consisted of **MO** and cationic lipid **DOTAP**, were used to encapsulate the antibiotic rifampicin (Rif). The positive charge of **DOTAP** is believed to improve the interaction of the nanoparticles with bacterial membranes, thereby enhancing the effectiveness of the antibiotic. Rif is a poorly soluble antibiotic used to treat infections including *S. aureus*, MRSA, and *Mycobacterium tuberculosis*.[58] In some patients, Rif can display a number of side effects including fever, hepatotoxicity, gastrointestinal irritation, and adverse immune responses. Its poor water solubility and side effects make this drug an ideal candidate for incorporating in a nano formulation. Prior research has shown that Rif-loaded liposomes display anti-biofilm activity against *Staphylococcus epidermidis in vitro*.[59] Other researchers have shown an improvement in the antibacterial effect of Rif-loaded solid lipid nanoparticles compared to free Rif *in vitro*.[60] Few studies have reported results with data conducted using *in vivo* experiments and none using lyotropic liquid crystal forming lipids. In our study, the **NanoRIF** formulation was tested against MRSA *in vitro* and *in vivo* in an infected wound model in mice. For the first time, we have also investigated the interactions of non-lamellar lipid nanoparticles with *S. aureus* using cryogenic transmission electron microscopy (cryo-TEM) showing strong interactions between the nanoparticles and the bacteria.

2. Materials and methods

2.1 Materials

MO was obtained from Nu-chek Prep Inc., (MN, USA) with purity >99%. 1,2-Di-oleyl-3 trimethyl-ammonium-propane (**DOTAP**) (purity > 99%) was purchased from Avanti Polar Lipids, (AL, USA). Pluronic F127 and Rif (purity > 97%) were purchased from Sigma Aldrich (**MO**, USA) and used as received. The structures of **MO**, Rif, **DOTAP** and a schematic representation of the lipid mesophase nanoparticle structure formed by mixing these components is presented in Fig. 1.

2.2 Lipid nanoparticle formulation

MO and **DOTAP** solutions were prepared separately in ethanol while Rif was dissolved in chloroform. Rif and **DOTAP** weights were prepared at 10% and 5% of total lipid weight respectively (**NanoRIF**). Mixtures of **MO** with 10% Rif (**MO-RIF**) and **MO** with 5% **DOTAP** (**MO-DOTAP**) were also prepared for comparison. Solvents were then evaporated overnight using a centrifugal evaporator (GeneVac EZ-2, NSW, Australia) or a high speed evaporating system (CombiDancer, NSW, Australia). Pluronic F127 solutions (500 μL) in Milli-Q water were added to the lipid mixtures. The Pluronic F127 weight was kept at 10 wt% of lipid throughout the study. Mixtures were then sonicated by using a multi-probe high throughput sonicator (QSonica Q700, Newtown, CT, USA) at 30% amplitude, with a 5 s on, 5 s-off mode for a total of 3 min. The plate was then sealed, and the resultant dispersions were kept at room temperature for further

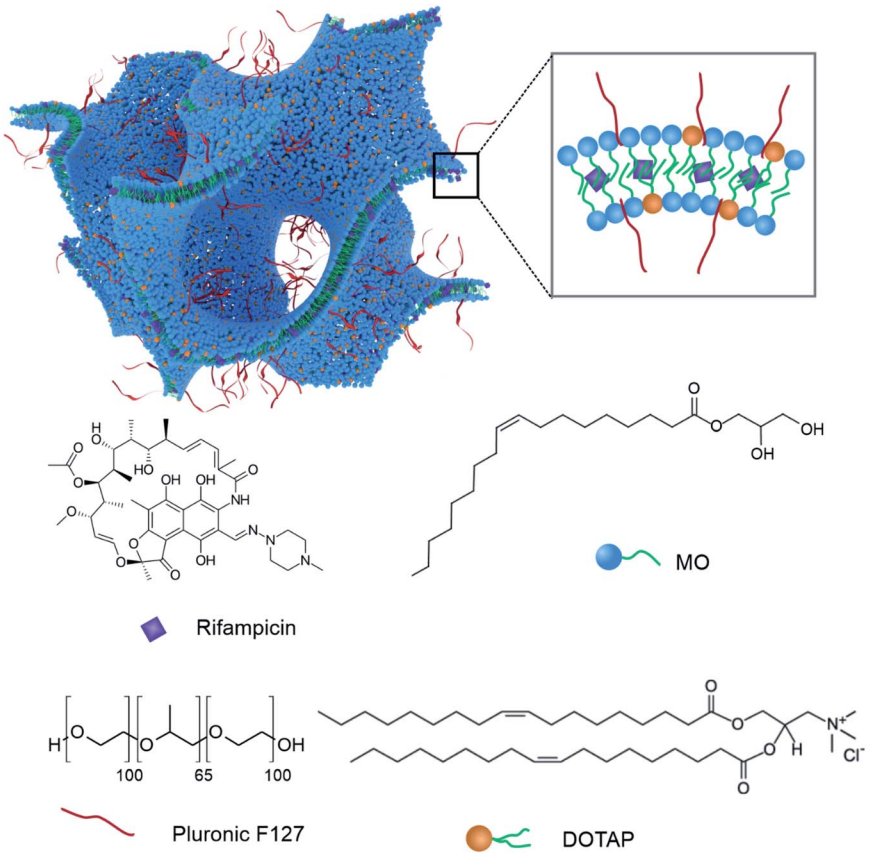

Fig. 1 Molecular structures of the compounds used to produce the antibacterial nanoparticles including MO, DOTAP and Rifampicin. Once these compounds are mixed together to form a gel, nanoparticles are formed *via* sonication with the addition of water or buffer containing Pluronic F127.

examination. The composition of each sample is summarised in Table 1. Throughout the study, the nanoparticle concentration refers to the concentration of lipid, which included **MO** and/or **DOTAP**.

2.3 Nanoparticle characterisation

2.3.1 Cryogenic transmission electron microscopy (Cryo-TEM). Cryo-TEM was used to visualize the formed nanoparticles. Copper grids (200 mesh) coated with perforated carbon film (Lacy carbon film: ProSciTech, Qld, Australia) were glow discharged for 60 seconds in a Pelco easiGlow (Ted Pella, USA) to render them hydrophilic and then placed in a laboratory-built humidity-controlled vitrification system. The dispersions were aspirated several times to ensure good mixing, then a droplet was placed onto the grids which were gently blotted by filter paper for approximately 3 s and then immediately plunged into liquid ethane cooled by liquid nitrogen. The samples were examined using a Gatan 626 cryoholder (Gatan, Pleasanton, CA, USA) and Tecnai 12 Transmission Electron Microscope (FEI, Eindhoven, The Netherlands) at an operating voltage of 120 kV, beam dose was kept below 10 electrons per $Å^2$. Images were recorded using a FEI Eagle 4k × 4k CCD camera at magnification ranging from 15 000 to 42 000.

2.3.2 Dynamic light scattering (DLS). Nanoparticle hydrodynamic diameters and the particle size distribution (polydispersity index – PdI) were measured by DLS using DynaPro Plate Reader (Wyatt Technology Co., Santa Barbara, CA, USA). For this, nanoparticles were diluted to 0.5 mg mL^{-1}. Samples were analysed with Dynamics software at 25 °C using a refractive index of 1.33. Milli-Q Water (18.2 MΩ) was used as the

Table 1 Composition of MO-based lipid nanoparticles used in this study including control nanoparticles and those containing DOTAP and Rif

Sample code	**MO** (mg)	Rif (mg)	**DOTAP** (mg)	Pluronic F127 (mg)
MO	10	0	0	1
MO-RIF	10	1	0	1
MO-DOTAP	9.5	0	0.5	1
MO-DOTAP-RIF (NanoRIF)	9.5	1	0.5	1

solvent to calculate the hydrodynamic sizes of the nanoparticles. Triplicate measurements with a minimum of 5 runs were performed.

2.4 Bacterial characterisation

2.4.1 Bacterial minimum inhibitory concentration (MIC) assay. An inoculum of *S. aureus* MRSA strain (ATCC1698) was prepared by transferring a colony directly from a nutrient agar plate into 10 mL of Tryptic Soy Broth (TSB) bacterial growth media, and grown overnight at 37 °C. The density of the bacteria was measured and adjusted to approximately 1×10^8 cfu mL^{-1} (colony forming units per mL) with an OD_{600} value of approximately 1. The bacterial suspension was then diluted to 1×10^5 cfu mL^{-1} in TSB media. Serial two-fold dilutions of the lipid nanoparticles in Milli-Q water were prepared to obtain the desired concentration range. An aliquot of 50 μL of the nanoparticle solution was added into each well of a sterile Nuclon® 96-well plate containing 50 μL of the bacterial suspension in triplicate. Positive controls contained only an aliquot of the bacterial suspension and Milli-Q water (growth control) and negative control wells contained TSB medium and the nanoparticles. The plates were incubated at 37 °C for 24 h while under constant shaking at 75 rpm.

The MIC was defined as the lowest concentration of the sample that completely inhibited the growth of the bacteria. In this study, to determine MIC, absorbance measurements were made with a 96-well plate reader (Wallac 1420, PerkinElmer) after 0 h and 24 h. The value at 0 h was subtracted from the value at 24 h in order to correct for background. The experiments were performed three times and the data was reported as mean ± standard deviation.

2.4.2 Mouse model of *S. aureus* infected surgical wound. The *S. aureus* MRSA strain (ATCC1698) was cultured at 37 °C on brain heart infusion (BHI) agar plates, or in BHI broth (Oxoid, UK). The number of bacteria was determined by measuring the optical density at 590 nm of an overnight culture, where OD 1.0 was previously determined to equivalent to 10^9 cfu per mL.

Female 8–10 week-old C57BL/6 mice (ARC, Perth, Australia) were housed in IVC cages under SPF conditions. Food and water were available *ad libitum*. All experiments were performed with the approval of the RMIT Animal Ethics committee (approval numbers 1728 and 1817).

For surgery, mice were induced and maintained under anaesthesia with inhaled isoflurane. The surgical site on the dorsal area was shaved and disinfected with 70% ethanol. After site preparation, Bupivacaine (0.25%) was injected subcutaneously in a line block for local anaesthesia. A 10 mm incision was made in the dorsal skin, and a subcutaneous pocket approx. 10 mm long was formed using scissor tips. Ten 10 μL of a suspension 10^8 *S. aureus*, or sterile saline was pipetted into the base of the subcutaneous pocket and the wound was closed with either sutures (Ethibond 6.0, Ethicon US LLC) or a stainless-steel staple (Reflex 7, Cell Point Scientific, Gaithersburg, MD). After wound closure, **NanoRIF**, Rifampicin alone (**RIF**), **MO-DOTAP**, **DOTAP** alone or sterile saline as a control were injected subcutaneously into the wound site. Mice were housed individually after surgery. Mice were weighed before surgery, and daily until day 5. Assessment of health status was made twice daily and clinical scores were recorded using the scoring system shown in Table 2.

Mice were killed on day 1 and 5, after euthanasia, 10 mm^2 skin including the wound site was dissected away, and half was used for determination of *S. aureus* colonisation, histology or FACS analysis as required. For determination of *S. aureus* colonisation, skin was collected into pre-weighted tubes containing 2 mL BHI. Tissue was homogenised and 100 μL was plated out onto selective BHI agar containing (1.5 μg mL^{-1} Oxacillin, 12.5 μg mL^{-1} Ampicillin, 2 μg mL^{-1} Polymixin B). Colonies were counted after 24 hours at 37 °C and data are expressed as cfu g^{-1} skin.

2.4.3 Flow cytometry. For flow cytometry analysis skin was collected into ice cold DMEM medium (Gibco BRL) containing 2% FCS. Lymphocytes were isolated from skin using collagenase/dispase treatment as described in.[61] After blocking Fc receptor sites, cell suspensions were stained with ZombieAqua (Biolegend), and then with a cocktail of surface markers: CD45, CD3, CD4, CD8, CD11b, Ly6G (all from Biolegend). Single-stained cytometric beads were used as compensation controls and labelled non-specific isoform control antibodies as negative controls (Biolegend). Stained were cells were washed and acquired using a FACSCanto II with FACsDiva (Becton Dickinson), analysis was performed using FlowJo software (V10.4.3, FLowJo Treestar, LLC). Cells were gated to exclude dead cells and aggregates, and gating was applied to detect lymphocytes based on FSC ad SSC characteristics. Inflammatory cell populations were defined as follows: neutrophils ($CD45^+$, $CD3^-$, $CD11b^+$, $Ly6G^+$), macrophages ($CD45^+$, $CD3^-$, $CD11b^+$), $CD4^+$ T cells ($CD45^+$, $CD3^+$, $CD4^+$).

Statistical analysis was performed using GraphPad Prism (V8.0.1, GraphPad Software Inc.). Datasets were tested for normality (D'Agostino & Pearson test), and because data for

Table 2 Criteria used to determine clinical scores in mice with *S. aureus* infected surgical wounds. Mice with scored 2 were monitored with increased frequency, any mouse meeting the criteria of score 3 was humanely killed

Response	Criteria	Clinical score
Mild	Weight loss < 10%	1
	Physical appearance	1
	Measurable clinical signs	1
	Behaviour (unprovoked)	1
	Behaviour (external stimuli)	1
Moderate	Weight loss > 10%	2
	Physical appearance	2
	Measurable clinical signs	2
	Behaviour (unprovoked)	2
	Behaviour (external stimuli)	2
Severe	Weight loss > 10%	≥3
	Physical appearance	≥3
	Measurable clinical signs	≥3
	Behaviour (unprovoked)	≥3
	Behaviour (external stimuli)	≥3

some groups were found not to be normally distributed, groupwise comparisons to untreated controls were made using the non-parametric Kruskal–Wallis test with Dunn's correction for multiple comparisons. Specific groups were also compared using a 2-tailed Mann–Whitney *U*-test as indicated. A value of P of 0.05 was considered significant.

3. Results

3.1 Characterization of MO based self-assembled lipid nanoparticles

A full detailed characterisation of the nanoparticles used in this work have been reported previously.[52] In our previous work, the composition of the nanoparticles was screened to obtain well dispersed colloidally stable nanoparticles. Briefly, **MO** nanoparticles were formed with Rif and **DOTAP** according to the ratios listed in Table 1. Visually, the nanoparticles are milky white dispersions in the absence of Rif but turn red in its presence. We have previously observed in nanoparticles containing both **DOTAP** and **RIF** (**NanoRIF**), a dramatic change in the SAXS profile. A single broad and strong peak with a maxima at around $q = 0.14$ Å^{-1} is observed. This is likely due to the presence of several co-existing intermediate phases including bicontinuous cubic and sponge phase, which has been confirmed by cryo-TEM.[62,63] It appears that the **MO** bilayer swells within the cubic phase to the point where long range order is lost. The hydrodynamic diameters of the nanoparticles in PBS were measured by DLS and are typically in the range from 150 nm to 230 nm. The zeta potential of the **MO** nanoparticles is almost neutral as expected ($\zeta = -1.2 \pm 0.1$ mV). Addition of Rif to the **MO** nanoparticles results in them being slightly more negatively charged ($\zeta = -4.1 \pm 0.4$ mV) whilst the **NanoRIF** particles exhibit a zeta potential of 25.5 ± 0.4 mV.

We previously reported enhanced interactions of these cationic charged nanoparticles with the negatively charged bacteria *via* electrostatic forces. No direct visual observation of this interaction was possible however fluorescent confocal microscopy confirmed colocalization of the **NanoRIF** with *S. aureus* bacteria. Additionally, Forster resonance energy transfer (FRET) analysis of **NanoRIF** in the presence of *S. aureus* suggested fusion between the nanoparticles and bacterial cell walls occurred. In this work we postulated that the capturing of direct interactions with *S. aureus* and **NanoRIF** *via* the use of cryo-TEM may be possible. Therefore, we undertook a systematic and thorough investigation of various experimental conditions in order to attempt this.

3.2 Cryo-TEM analysis of interactions of NanoRIF with MRSA

From the antimicrobial activity data presented in our previous work, it was clear that the presence of **DOTAP** enhanced the antibacterial effect of Rif towards *S. aureus in vitro*. We observed

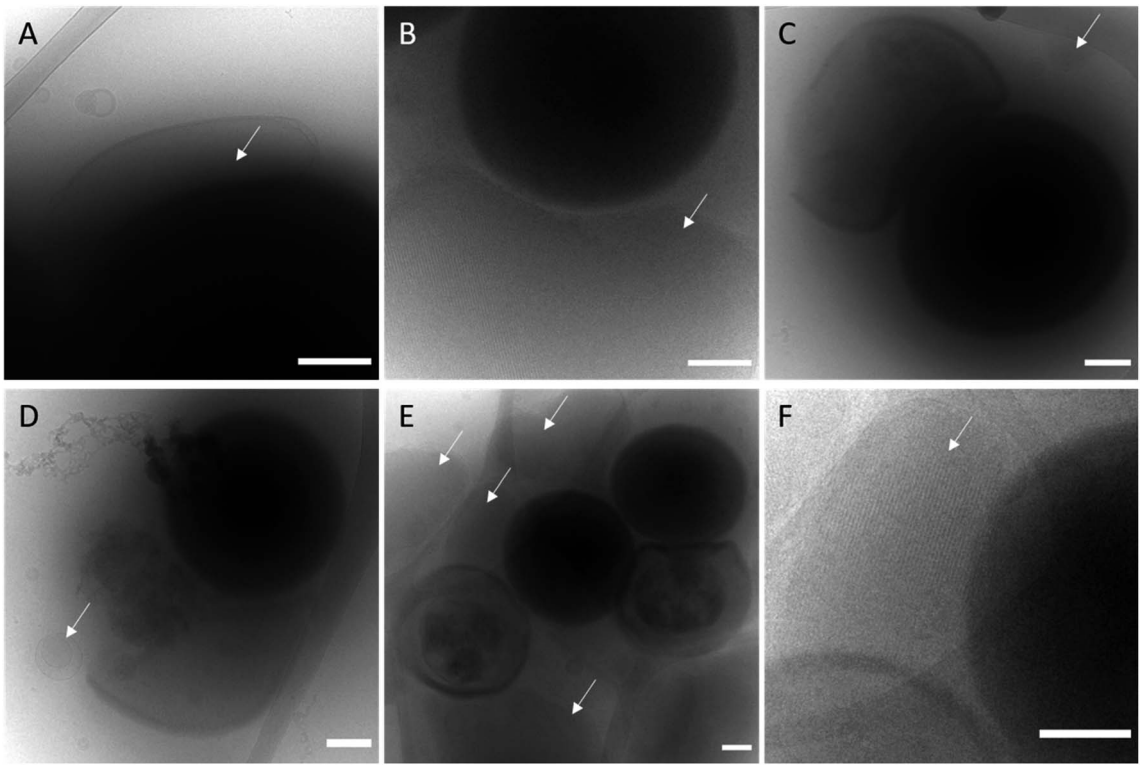

Fig. 2 NanoRIF particles can be seen interacting with *S. aureus*. (A and B) After 1 hour incubation, NanoRIF particles are in close proximity to *S. aureus*. and are conforming to the contours of the cells. After 2 (C), 4 (D) and 5 (E) hours a mixture of live and dead *S. aureus* is observed. Ruptures in cell membranes are evident. (F) A close crop taken from (E) showing the structure of the nanoparticle, and its proximity to the bacteria. White arrows indicate the location of NanoRIF particles. Scale bars are 200 nm.

co-localisation of **NanoRIF** using FRET fluorophores indicating that they either bind to or fuse with the bacteria. It was clear that these co-localisation events occurred more frequently with the **NanoRIF** nanoparticles than for **MO-RIF** nanoparticles. This increased membrane binding of **MO-DOTAP-RIF** to the *S. aureus* indicates that the positive charge of the **DOTAP** containing nanoparticles promotes electrostatic binding with the negative charge present at the surface of the bacteria. We hypothesise that these binding and possible fusion events, which are likely enhanced by the presence of the cationic lipid **DOTAP**, may have boosted the delivery of Rif into the bacteria, leading to greater cell death and improved efficacy of the antibiotic Rif. We were interested to attempt to visualise these interactions to see if any evidence of membrane fusion was evident which is a reported mechanism for drug loaded liposomes incubated *in vitro* with *S. aureus*, *Stenotrophomonas maltophilia*, and *Propionibacterium acnes*.[64,65]

In order to attempt to visualize the effect that **DOTAP** had on nanoparticle-bacteria interactions, cryo-TEM was used. Remarkably we have been able to show strong interactions of the **NanoRIF** with *S. aureus* using cryo-TEM after some trial and error in perfecting the experimental protocols. It was important to vortex mix the bacterial-nanoparticle solutions immediately prior to blotting of the samples for vitrification on the lacey carbon grids. The images in Fig. 2A and B clearly show strong interactions where lamellar and cubic phase displaying nanoparticles are enveloping the spherical bacteria. In Fig. 2A, an ovular lipid nanoparticle rests on top of a *S. aureus* bacterium whilst in Fig. 2B, a cubic phase nanoparticle can clearly be seen enveloping a bacterium from below. Fig. 2C–E show ruptured bacteria, healthy bacteria and cubic phase nanoparticles (white arrows) in close location. The nanostructure of the particles is visible in the high resolution image in Fig. 2F, confirming the presence of a cubic phase.

The complete destruction of *S. aureus* cell membranes is evident in the cryo-TEM images however no evidence of membrane fusion, rather membrane binding events were observed. The cryo-TEM data indicates that the nanoparticles carrying Rif have caused membrane damage leading to cell death. It is likely that membrane fusion events do occur, but we have been unable to capture a fusion event in this experiment. In a recent work, Conn *et al.* have provided evidences of membrane fusion events between cubosomes and model lipid bilayers.[66] Additionally, a work by Boge *et al.* showed evidence of fusion between antimicrobial peptide loaded lipid nanoparticles and *E. coli* using cryo-TEM.[67] Whether or not this is occurring in our system with *S. aureus* is yet to be determined.

3.3 *In vitro* antibacterial properties of NanoRIF against MRSA

In our previous work we reported the toxicity and minimum inhibitory concentration (MIC) concentrations for **NanoRIF** against *S. aureus* (ATCC 29213) and observed that the MIC of **NanoRIF** was lower than the free drug (**RIF**). Here we extended the studies to a *S. aureus* MRSA strain (ATCC1698) and tested the efficacy of **NanoRIF** both *in vitro* and *in vivo* in a skin wound infection model. The results of the *in vitro* MIC testing conducted are summarised in Table 3. It can be seen that, **MO** nanoparticles and **MO-DOTAP** nanoparticles did not show any antibacterial activity against *S. aureus* 1698. The MICs of all Rif containing formulations, *i.e.* **MO-RIF** and **NanoRIF**, were however similar to that of the free Rif control and were around 0.025 μg mL^{-1}. These data suggest that at least *in vitro*, the impact of nanoparticle formulations containing Rif may be strain-dependent.

Table 3 MIC values of MO-based nanoparticles loaded with Rif against MRSA strain (ATCC1698). MIC values were determined after 24 h growth in tryptic soy broth. While MO and MO-DOTAP nanoparticles had no significant antibacterial effect, the MIC for RIF was similar for both the nanoparticle and free drug. Data represent the average of 3 replicate experiments

Formulation	MIC (μg mL^{-1})
MO	>1.6
MO-DOTAP	>1.6
MO-RIF	0.025
NanoRIF (**MO-DOTAP-RIF**)	0.025
RIF (free Rif dissolved in DMSO)	0.025

3.4 NanoRIF is well tolerated and effective at reducing *S. aureus* colonization of infected wounds in mice

To investigate the antimicrobial activity of the components of **NanoRIF**, *S. aureus* infected surgical wounds were made in groups of mice (5 per group). Wounds were treated with **RIF** alone, **MO-DOTAP**, **MO-RIF**, **NanoRIF**, or sterile saline as control. Control mice had non-infected wounds. The dose of 25 mg kg^{-1} **NanoRIF** was determined to be well-tolerated in preliminary experiments (data not shown).

S. aureus colonisation and clinical scores were determined on day 1 ($n = 2$) and 5 ($n = 3$). As expected, saline control and **MO-DOTAP** alone did not reduce bacterial colonisation. In contrast, free **RIF**, **MO-RIF** and **NanoRIF** all reduced the number of *S. aureus* by approximately 2 and 5 log on day 1 and 5 respectively (Fig. 3). Although there was a tendency for control mice to lose more weight than treated mice, there was no significant difference in either clinical scores or weight at day 5 (Fig. 3C and D) ($p < 0.05$). It is noteworthy that the clinical score for all mice in the study was less than 1.5, and the score defining an intervention is 3 (Table 2). This is further evidence that **NanoRIF** formulations were safe and well-tolerated.

3.5 NanoRIF treatment significantly reduces *S. aureus* colonisation, at a reduced dose

In order to compare the efficacy of **NanoRIF** to **RIF** alone, groups of 10 mice received MRSA contaminated wounds as above, and were treated with saline, **NanoRIF** or free **RIF** at full (25 mg kg^{-1}) or reduced 12.5 mg kg^{-1} or 2.5 mg kg^{-1} Rif doses diluted in saline. Control mice had non-infected wounds. Weights, clinical scores and cfu count at the wound site were determined as previously, and immune cells in wound infiltrates were

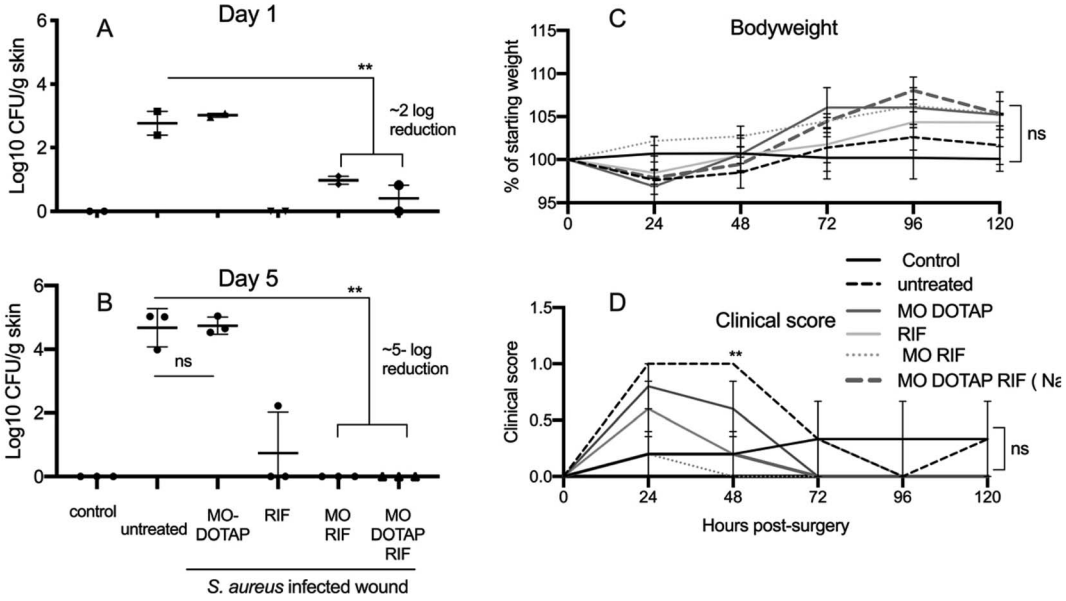

Fig. 3 NanoRIF is safe and effective at reducing *S. aureus* colonization of infected wounds. Surgical wounds were either non-infected (control) or infected with 10^8 *S. aureus* and treated with saline, MO-DOTAP, free RIF, MO-RIF or NanoRIF (MO-DOTAP-RIF). The number of *S. aureus* cfu was determined on days 1 (A) and 5 (B). No adverse effects were detected, and both bodyweight (C), and clinical scores (D) were similar for all treated mice. Treatment with MO-RIF and NanoRIF resulted in significant reduction or elimination of *S. aureus* from the wound site, whereas MO-DOTAP alone had no effect on colonization ($n = 2$, day 1, $n = 3$, day 5). Control untreated mice had higher clinical scores at 48 h post-surgery, but all treatment groups were similar by day 5. ** $p < 0.05$.

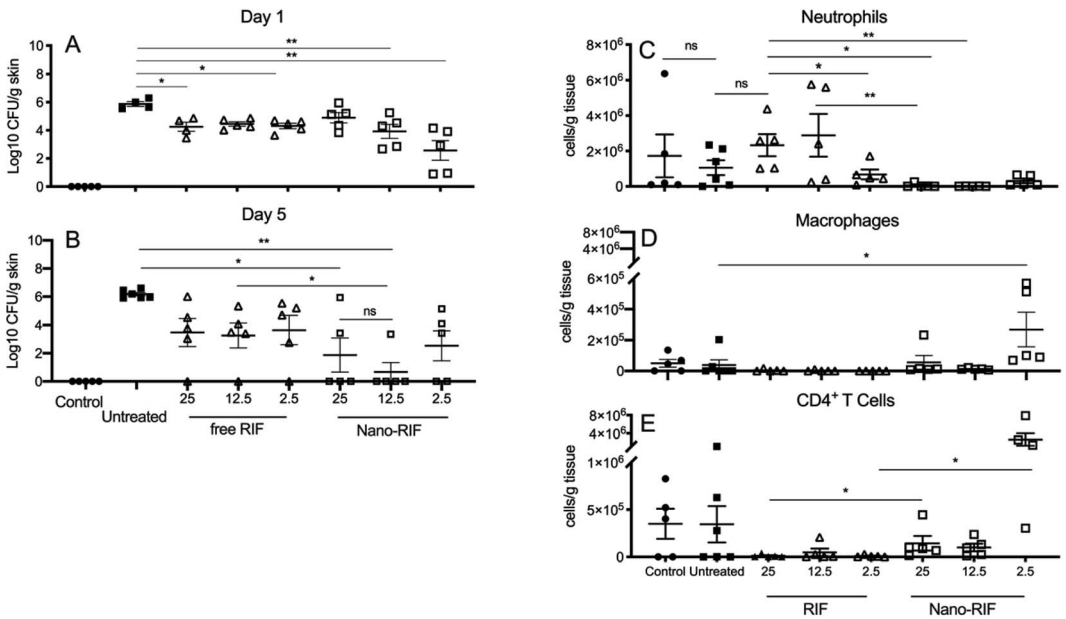

Fig. 4 Effect of reduced dose NanoRIF treatments on *S. aureus* colonization (A and B) and immune cell responses (C–E). Surgical wounds were either non-infected (control) or infected with 10^8 *S. aureus* and treated with saline (untreated), or different doses of RIF (25, 12.5 or 2.5 mg kg^{-1}) or NanoRIF (MO-DOTAP-RIF) (25, 12.5 or 2.5 mg kg^{-1}). The number of *S. aureus* cfu was determined on days 1 (A) and 5 (B). Most NanoRIF treated mice had significantly reduced or eliminated the infection by day 5 (* $p < 0.05$, ** $p < 0.001$). Lymphocytes were isolated from the wound site on day 5 ($n = 5$ per group) and stained for flow cytometry analysis of neutrophil (C), macrophage (D) and $CD4^+$ T (E) cells. Mice with wounds treated with NanoRIF had significantly lower numbers of neutrophils infiltrating the site (**$p < 0.005$,*$p < 0.01$) compared to RIF alone. Only the NanoRIF 2.5 mg kg^{-1} group had significantly more macrophages present than controls (*$p < 0.05$). Mice that received 25 and 2.5 mg kg^{-1} doses of NanoRIF had significantly more infiltrating $CD4^+$ T cells than those treated with equivalent doses of RIF alone (* $p < 0.05$, ** $p < 0.001$).

characterized by flow cytometry. Fig. 4 shows that while treatment with **RIF** alone did lead to reductions in *S. aureus* cfu count compared to untreated mice, there was no significant difference between the doses used. Further, by day 5, mice treated with 25 mg kg^{-1} **NanoRIF** had either significantly lower, or no detectable bacteria ($p < 0.05$) compared to untreated controls. The reduction was significant, but the fact that bacteria were detected in 2/5 mice in the 25 mg kg^{-1} treated mice means that overall reduction was less than observed in Fig. 3, this may reflect a technical issue such as unobserved leakage of the **NanoRIF** after injection to the wound site. Notably the 12.5 **NanoRIF** mg kg^{-1} dose was significantly better at reducing colonization that 12.5 mg kg^{-1} **RIF** alone, and 4/5 of the **NanoRIF** treated mice had no detectible bacteria at day 5 (Fig. 2B). The range of cfu obtained for the 2.5 mg kg^{-1} dose of **NanoRIF** was greater and only 2/5 had no bacterial count. All treatments were well-tolerated by mice and there was no significant difference in clinical scores or body weight between and treatment group compared to controls (data not shown). In summary, our data show that **NanoRIF** was more effective than free **RIF** at the 12.5 mg kg^{-1} dose.

3.6 NanoRIF treated mice have reduced numbers of neutrophils and increased numbers of $CD4^+$ T cells at wound sites

Lymphocytes were isolated from the wound site on day 5 ($n = 5$ per group) and stained for flow cytometry analysis of neutrophil, macrophage and $CD4^+$ T cells (Fig. 4C–E). Mice with wounds treated with **NanoRIF** had significantly lower numbers of neutrophils infiltrating the site compared to control mice, or those treated with an equivalent dose of free **RIF** ($p < 0.05$). A dose dependent effect was observed for **RIF** treated mice and those treated with 2.5 mg kg^{-1} had significantly fewer neutrophils than the 25 mg kg^{-1} treatment group ($P = 0.0317$, Mann–Whitney *U*-test, 2-tailed).

Overall low numbers of macrophages were detected at the wound sites in all groups, however the 2.5 mg kg^{-1} **NanoRIF** treated group had significantly higher numbers ($P = 0.0038$) compared to control groups. Overall, low numbers of $CD4^+$ T cells were detected in the wound infiltrates, however mice that received 12.5 and 2.5 mg kg^{-1} **NanoRIF** doses had significantly more infiltrating $CD4^+$ T cells than those treated with **RIF** alone ($P = 0.0079$ and 0.0159 respectively, Mann–Whitney *U*-test, 2-tailed).

4. Discussion

Cationic nanoparticles are attractive as potential vehicles to improve the stability and delivery of anti-microbial drugs, particularly those that are poorly soluble such as Rif. Rif is an antibiotic mainly used to treat infections with Gram-positive bacteria in humans and animals, and is a first-line drug used to treat tuberculosis.[68] Rif has also been used as an adjunct therapy to treat methicillin resistant *Staphylococcus aureus* (MRSA) infections due to its good tissue penetration compared to vancomycin.[69]

The efficacy of Rif for treatment of MRSA has been the subject to some controversy, and the recent ARREST clinical trial reported a small, but statistically non-significant enhancement of survival in patients with MRSA bloodstream infections who received Rif as adjunct therapy.[70] The same study reported that in the UK, an episode of severe systemic MRSA infection cost approximately £12 000, and that treatment with Rif reduced costs by 10%.[70] Rif has also been used extensively to treat orthopaedic and device-related infections, and patients treated with Rif combination therapy have cure rates of 80–100% compared to 30–60% for conventional regimes.[71]

Rif formulated into **MO-DOTAP** nanoparticles (**NanoRIF**) have previously been shown to have low toxicity for mammalian cells *in vitro*,[52] and a major aim of this study was to determine the safety and efficacy of **NanoRIF** in an *in vivo* model of *S. aureus* infection. The poor solubility of Rif in water, and its reported tissue irritant effects mean that Rif is usually applied either orally or intravenously, reducing its utility. Thus, a second aim of this study was to investigate the potential impact of **MO-DOTAP** on the tissue compatibility of Rif.

The mouse model of MRSA infected surgical wounds employed in this study provided an opportunity to study both the anti-microbial efficacy, and any local irritation caused by free **RIF** and **NanoRIF** *in vivo*. In this model, while all mice exhibit weight loss of approx. 5–10% in the first 24–48 h after surgery, mice with untreated wounds tended to exhibit more weight loss, and higher clinical scores. The beneficial effect was, however, generally not significantly different for mice treated with free **RIF** or **NanoRIF**.

Initially we tested several formulations containing a high dose of 25 mg kg^{-1} of Rif and observed that all mice treated with free **RIF**, **MO-RIF** or **NanoRIF** tended to gain more weight, and better recovery (as evidenced by lower clinical scores) than untreated controls, although this was not statistically significant (Fig. 3C and D). Treatment with **MO-RIF** or **NanoRIF** had significantly reduced colonisation with *S. aureus* to undetectable levels in all 3 mice by day 5, whereas 1 of 3 **RIF** treated mice still had detectable bacteria present (Fig. 3A and B). Consistent with our previous *in vitro* studies, **MO-DOTAP** alone had no antibacterial effect.[52]

The larger study confirmed our initial findings on the anti-microbial effects of **NanoRIF** and showed that the reduced doses of 12.5 mg kg^{-1} and 2.5 mg kg^{-1} also significantly reduced *S. aureus* colonisation compared to untreated, and **RIF** 12.5 mg kg^{-1} treated wounds (Fig. 4B). Formulating **RIF** with **MO-DOTAP**, thus appears to enhance its antimicrobial activity *in vivo* when using MRSA but does not improve its efficacy when tested *in vitro*. The enhancing effect on anti-microbial activity *in vivo* may possibly be due to effects of the cationic particles 'targeting' the bacterial cell wall that were previously reported[52] which may aid in potentiating the access of **RIF** to bacterial membranes.

Cationic particles are also known to be taken up by immune cell populations, and to cause inflammation in their own right,[72,73] it was therefore important to investigate the impact of these effects on the ability to clear an infection *in vivo*. As discussed above, Rif is not usually administered *via* the subcutaneous route due to reported tissue irritation. In this study only

the highest dose of 25 mg kg^{-1} Rif showed evidence of mild local irritation as evidenced by an infiltrate of neutrophils that was similar to the local *S. aureus* infection (Fig. 4C). Neutrophils are the primary innate cell population that enter wounds in response to tissue damage and infection and are important for bacterial killing and attracting other immune cells to a site of infection. Although in our experiments, no significant irritation was observed macroscopically on any wound site, an extremely interesting finding of this study was that the number of neutrophils detected in the wound sites of **NanoRIF** treated mice was significantly lower than in **RIF** or untreated mice (Fig. 2C). This is of particular interest because the *in vivo* antibacterial effects were greatest in mice treated with **NanoRIF**. This finding indicates the nanoparticles themselves may be aiding in the host defense response to the infection from the MRSA bacteria and potentially having an adjuvant effect.[74]

Neutrophils and macrophages are the main cells that responsible to the wound healing process. Without an ongoing infection, neutrophil activity should gradually decrease. Prolonged neutrophil activity may indicate delayed wound healing and can result in tissue damage.[75,76] It is possible that the enhanced killing that we have observed was a result of the membrane damaging effects of **NanoRIF**, and this may have resulted in quicker clearance of the wound sites, and thus fewer neutrophils by day 5. The implications of the increased numbers of $CD4^+$ T-cells and macrophages in mice treated with the low dose of **NanoRIF** require further investigation. $CD4^+$ T-cells generally direct adaptive immune response and provide help to promote the development of antibody responses for example. A study of specific antibody responses was beyond the scope of this study in an acute infection model, but **DOTAP** containing lipid nanoparticles have previously been reported to have adjuvant effects in experimental vaccine studies.[77] Macrophages and T cells are likely to have been attracted to the site of the **NanoRIF** depot as a result of local chemokine gradients. The mechanism for this is proposed to be due to enhanced membrane interactions with antigen presenting cells such as dendritic cells and macrophages. Future investigations should include an assessment of DC activation at earlier time points after administration.

In this study, **NanoRIF** was injected adjacent to the site of infection for an assessment of safety and antibacterial activity. Assessment of the EPR effect was therefore beyond the scope of this work. In future studies, the potential targeting of **NanoRIF** from a distant site would be of great interest, due to its potential for treatment of systemic infections, or infections in internal organs. Additionally, it would be of interest to investigate topical skin infections with this type of treatment. Taken together, our data suggest that the **NanoRIF** formulation reduces the dose required to clear a localised infection *in vivo*, and also reduces the tissue toxicity of Rif, potentially enhancing its utility for tissue infections.

5. Conclusion

In this work we have shown that **MO** lipid nanoparticles containing cationic lipid **DOTAP** and loaded with Rif (**NanoRIF**) are more effective at treating MRSA infection in a wound model in mice than the **RIF** alone. Interestingly, when the **NanoRIF** formulation was tested *in vitro* against MRSA it was found that the effect of free **RIF** *vs.* **NanoRIF** as measured by the minimum inhibitory concentration is similar. When *S. aureus* was incubated with the nanoparticles *in vitro*, strong interactions between the bacteria and nanoparticles are visible using cryo-TEM. An extremely interesting finding of this study is that the number of neutrophils detected in the wound site when using **NanoRIF** was significantly lower than when the free drug was used or when compared to the untreated mice control group. Our data suggests that the **NanoRIF** formulation reduces the dose required to clear a localised infection *in vivo*, reducing the tissue toxicity of Rif and potentially facilitates the immune system response enhancing its utility for tissue infections. The new findings we highlight here exemplify the concept of using lipid nanocarriers as drug delivery vehicles for the targeted treatment of infection *in vivo* and take the approach one step closer to a potential clinical treatment option. This work significantly enhances the potential of this approach and shows that additional benefits may exist when delivering antibiotics to infected wounds *in vivo* due to improved immune responses in addition to delivery of poorly soluble antibacterial compounds. This technique appears to be a useful method to enable and enhance the use of poorly soluble antibiotic drugs. Further research into this type of approach should enable the development of new strategies in the fight against multi-drug resistant strains of bacteria in various wound infection types.

Conflicts of interest

The authors declare no conflict of interest.

Acknowledgements

B. M. gratefully acknowledges funding through his CSIRO Office of the Chief Executive (OCE) Julius Career Award to conduct this research. N. T. is supported by a RMIT VC Research Fellowship. AW is supported by start-up funds from RMIT. The authors thank Mr Wil Gardner for assistance with rendering the cubic phase schematic image in Blender 2.81a.

References

1 B. Khameneh, R. Diab, K. Ghazvini and B. S. F. Bazzaz, Breakthroughs in bacterial resistance mechanisms and the potential ways to combat them, *Microb. Pathog.*, 2016, **95**, 32–42.
2 C. L. Ventola, The antibiotic resistance crisis: part 1: causes and threats, *Clin. Pharm. Ther.*, 2015, **40**(4), 277.
3 S. Wang, A. K. Singh, D. Senapati, A. Neely, H. Yu and P. C. Ray, Rapid Colorimetric Identification and Targeted Photothermal Lysis of Salmonella Bacteria by Using Bioconjugated Oval-Shaped Gold Nanoparticles, *Chem. - Eur. J.*, 2010, **16**(19), 5600–5606.
4 J. S. Molton, P. A. Tambyah, B. S. Ang, M. L. Ling and D. A. Fisher, The global spread of healthcare-associated

multidrug-resistant bacteria: a perspective from Asia, *Clin. Infect. Dis.*, 2013, **56**(9), 1310–1318.

5 H. C. Maltezou, Metallo-β-lactamases in Gram-negative bacteria: introducing the era of pan-resistance?, *Int. J. Antimicrob. Agents*, 2009, **33**(5), 405.e1–405.e7.

6 L.-C. Kuo, L.-J. Teng, C.-J. Yu, S.-W. Ho and P.-R. Hsueh, Dissemination of a clone of unusual phenotype of pandrug-resistant Acinetobacter baumannii at a university hospital in Taiwan, *J. Clin. Microbiol.*, 2004, **42**(4), 1759–1763.

7 H. W. Boucher, Challenges in anti-infective development in the era of bad bugs, no drugs: a regulatory perspective using the example of bloodstream infection as an indication, *Clin. Infect. Dis.*, 2010, **50**(Supplement_1), S4–S9.

8 A. Simon, M. L. A. Moreira, I. Costa, V. P. de Sousa, C. R. Rodrigues, L. Lima, T. Sisnande, F. A. do Carmo, I. C. R. Leal, K. R. N. dos Santos, L. da Silva and L. M. Cabral, Vancomycin-loaded nanoparticles against vancomycin intermediate and methicillin resistantStaphylococcus aureusstrains, *Nanotechnology*, 2020, **31**(37), 9.

9 H. J. Stacey, C. S. Clements, S. C. Welburn and J. D. Jones, The prevalence of methicillin-resistant Staphylococcus aureus among diabetic patients: a meta-analysis, *Acta Diabetol.*, 2019, **56**(8), 907–921.

10 A. Parisi, M. Caruso, G. Normanno, L. Latorre, A. Miccolupo, R. Fraccalvieri, F. Intini, T. Manginelli and G. Santagada, MRSA in swine, farmers and abattoir workers in Southern Italy, *Food Microbiol.*, 2019, **82**, 287–293.

11 J. Kim, B. E. Kim, K. Ahn and D. Y. M. Leung, Interactions Between Atopic Dermatitis and Staphylococcus aureus Infection: Clinical Implications, *Allergy, Asthma Immunol. Res.*, 2019, **11**(5), 593–603.

12 R. Dotel, M. V. N. O'Sullivan, J. S. Davis, P. J. Newton and G. L. Gilbert, Molecular epidemiology of methicillin-resistant Staphylococcus aureus isolates in New South Wales, Australia, 2012-2017, *Infection, Disease & Health*, 2019, **24**(3), 134–140.

13 K. Bush, P. Courvalin, G. Dantas, J. Davies, B. Eisenstein, P. Huovinen, G. A. Jacoby, R. Kishony, B. N. Kreiswirth and E. Kutter, Tackling antibiotic resistance, *Nat. Rev. Microbiol.*, 2011, **9**(12), 894.

14 S. J. Rehm and A. Tice, Staphylococcus aureus: Methicillin-Susceptible S. aureus to Methicillin-Resistant S. aureus and Vancomycin-Resistant S. aureus, *Clin. Infect. Dis.*, 2010, **51**, S176–S182.

15 S. Rieg, G. Peyerl-Hoffmann, K. de With, C. Theilacker, D. Wagner, J. Hubner, M. Dettenkofer, A. Kaasch, H. Seifert, C. Schneider and W. V. Kern, Mortality of S. aureus bacteremia and infectious diseases specialist consultation – a study of 521 patients in Germany, *J. Infect.*, 2009, **59**(4), 232–239.

16 X. Zhu, A. F. Radovic-Moreno, J. Wu, R. Langer and J. Shi, Nanomedicine in the management of microbial infection–overview and perspectives, *Nano today*, 2014, **9**(4), 478–498.

17 K. Thakur, G. Sharma, B. Singh, S. Chhibber and O. P. Katare, Nano-engineered lipid-polymer hybrid nanoparticles of fusidic acid: an investigative study on dermatokinetics profile and MRSA-infected burn wound model, *Drug Delivery Transl. Res.*, 2019, **9**(4), 748–763.

18 A. J. Huh and Y. J. Kwon, "Nanoantibiotics": a new paradigm for treating infectious diseases using nanomaterials in the antibiotics resistant era, *J. Controlled Release*, 2011, **156**(2), 128–145.

19 B. Singh, P. R. Vuddanda, M. R. Vijayakumar, V. Kumar, P. S. Saxena and S. Singh, Cefuroxime axetil loaded solid lipid nanoparticles for enhanced activity against S. aureus biofilm, *Colloids Surf., B*, 2014, **121**, 92–98.

20 J. Jampilek and K. Kral'ova, *Nanoantimicrobials: Activity, Benefits, and Weaknesses*, 2017, pp. 23–54.

21 M. Ramos, P. B. Da Silva, L. Sposito, L. G. De Toledo, B. V. Bonifacio, C. F. Rodero, K. C. Dos Santos, M. Chorilli and T. M. Bauab, Nanotechnology-based drug delivery systems for control of microbial biofilms: a review, *Int. J. Nanomed.*, 2018, **13**, 1179–1213.

22 R. Duncan, The dawning era of polymer therapeutics, *Nat. Rev. Drug Discovery*, 2003, **2**(5), 347.

23 E. A. Azzopardi, E. L. Ferguson and D. W. Thomas, The enhanced permeability retention effect: a new paradigm for drug targeting in infection, *J. Antimicrob. Chemother.*, 2012, **68**(2), 257–274.

24 P. Laverman, O. C. Boerman, W. J. Oyen, E. T. M. Dams, G. Storm and F. H. Corstens, Liposomes for scintigraphic detection of infection and inflammation, *Adv. Drug Delivery Rev.*, 1999, **37**(1), 225–235.

25 P. Laverman, O. C. Boerman, W. J. Oyen, F. H. Corstens and G. Storm, In vivo applications of PEG liposomes: unexpected observations, *Crit. Rev. Ther. Drug Carrier Syst.*, 2001, **18**(6), 551–566.

26 D. J. Evans, D. G. Evans and S. L. Gorbach, Production of vascular permeability factor by enterotoxigenic Escherichia coli isolated from man, *Infect. Immun.*, 1973, **8**(5), 725–730.

27 R. Labruere, A. J. Sona and E. Turos, Anti-Methicillin-Resistant Staphylococcus aureus Nanoantibiotics, *Front. Pharmacol.*, 2019, **10**, 24.

28 C. Sikkink, M. Reijnen, P. Laverman, W. J. G. Oyen and H. van Goor, Tc-99m-PEG-Liposomes Target Both Adhesions and Abscesses and Their Reduction by Hyaluronate in Rats With Fecal Peritonitis, *J. Surg. Res.*, 2009, **154**(2), 246–251.

29 U. Fiedler and H. G. Augustin, Angiopoietins: a link between angiogenesis and inflammation, *Trends Immunol.*, 2006, **27**(12), 552–558.

30 P. Laverman, E. T. M. Dams, G. Storm, T. G. Hafmans, H. J. Croes, W. J. Oyen, F. H. Corstens and O. C. Boerman, Microscopic localization of PEG-liposomes in a rat model of focal infection, *J. Controlled Release*, 2001, **75**(3), 347–355.

31 M. N. Swartz, Cellulitis – Reply, *N. Engl. J. Med.*, 2004, **350**(24), 2523–2524.

32 J. Zhang, Y. P. Chen, K. P. Miller, M. S. Ganewatta, M. Bam, Y. Yan, M. Nagarkatti, A. W. Decho and C. Tang, Antimicrobial metallopolymers and their bioconjugates with conventional antibiotics against multidrug-resistant bacteria, *J. Am. Chem. Soc.*, 2014, **136**(13), 4873–4876.

33 C. Fong, T. Le and C. J. Drummond, Lyotropic liquid crystal engineering–ordered nanostructured small molecule amphiphile self-assembly materials by design, *Chem. Soc. Rev.*, 2012, **41**(3), 1297–1322.

34 B. W. Muir, D. P. Acharya, D. F. Kennedy, X. Mulet, R. A. Evans, S. M. Pereira, K. L. Wark, B. J. Boyd, T. H. Nguyen, T. M. Hinton, L. J. Waddington, N. Kirby, D. K. Wright, H. X. Wang, G. E. Egan and B. A. Moffat, Metal-free and MRI visible theranostic lyotropic liquid crystal nitroxide-based nanoparticles, *Biomaterials*, 2012, **33**(9), 2723–2733.

35 C. V. Kulkarni, W. Wachter, G. Iglesias-Salto, S. Engelskirchen and S. Ahualli, Monoolein: a magic lipid?, *Phys. Chem. Chem. Phys.*, 2011, **13**(8), 3004–3021.

36 J. Seddon and R. Templer, Polymorphism of lipid–water systems, *Handbook of biological physics*, 1995, 1, pp. 97–160.

37 S. T. Hyde, Identification of lyotropic liquid crystalline mesophases, *Handbook of Applied Surface and Colloid Chemistry*, 2001, pp. 299–332.

38 J. M. Seddon and R. H. Templer, Polymorphism of lipid–water systems, *Handbook of Biological Physics*, 1995, 1, pp. 97–160.

39 D. Demurtas, P. Guichard, I. Martiel, R. Mezzenga, C. Hebert and L. Sagalowicz, Direct visualization of dispersed lipid bicontinuous cubic phases by cryo-electron tomography, *Nat. Commun.*, 2015, **6**, 8915.

40 G. L. Zhen, T. M. Hinton, B. W. Muir, S. N. Shi, M. Tizard, K. M. McLean, P. G. Hartley and P. Gunatillake, Glycerol Monooleate-Based Nanocarriers for siRNA Delivery in Vitro, *Mol. Pharm.*, 2012, **9**(9), 2450–2457.

41 N. Bye, O. E. Hutt, T. M. Hinton, D. P. Acharya, L. J. Waddington, B. A. Moffat, D. K. Wright, H. X. Wang, X. Mulet and B. W. Muir, Nitroxide-Loaded Hexosomes Provide MRI Contrast in Vivo, *Langmuir*, 2014, **30**(29), 8898–8906.

42 V. P. Torchilin, Multifunctional nanocarriers, *Adv. Drug Delivery Rev.*, 2012, **64**, 302–315.

43 V. P. Torchilin, Recent advances with liposomes as pharmaceutical carriers, *Nat. Rev. Drug Discovery*, 2005, **4**(2), 145–160.

44 H.-I. Chang and M.-K. Yeh, Clinical development of liposome-based drugs: formulation, characterization, and therapeutic efficacy, *Int. J. Nanomed.*, 2012, **7**(4), 49–60.

45 T. M. Allen and P. R. Cullis, Liposomal drug delivery systems: from concept to clinical applications, *Adv. Drug Delivery Rev.*, 2013, **65**(1), 36–48.

46 T. M. Hinton, F. Grusche, D. Acharya, R. Shukla, V. Bansal, L. J. Waddington, P. Monaghan and B. W. Muir, Bicontinuous cubic phase nanoparticle lipid chemistry affects toxicity in cultured cells, *Toxicol. Res.*, 2014, **3**(1), 11–22.

47 N. Tran, N. Bye, B. A. Moffat, D. K. Wright, A. Cuddihy, T. M. Hinton, A. M. Hawley, N. P. Reynolds, L. J. Waddington, X. Mulet, A. M. Turnley, M. C. Morganti-Kossmann and B. W. Muir, Dual-modality NIRF-MRI cubosomes and hexosomes: High throughput formulation and in vivo biodistribution, *Mater. Sci. Eng., C*, 2017, **71**, 584–593.

48 J. Zhai, J. A. Scoble, N. Li, G. Lovrecz, L. J. Waddington, N. Tran, B. W. Muir, G. Coia, N. Kirby and C. J. Drummond, Epidermal growth factor receptor-targeted lipid nanoparticles retain self-assembled nanostructures and provide high specificity, *Nanoscale*, 2015, **7**, 2905–2913.

49 A. Yaghmur, B. Sartori and M. Rappolt, Self-assembled nanostructures of fully hydrated monoelaidin–elaidic acid and monoelaidin–oleic acid systems, *Langmuir*, 2012, **28**(26), 10105–10119.

50 J. Borné, T. Nylander and A. Khan, Phase behavior and aggregate formation for the aqueous monoolein system mixed with sodium oleate and oleic acid, *Langmuir*, 2001, **17**(25), 7742–7751.

51 J. Zhai, C. Fong, N. Tran and C. J. Drummond, Non-lamellar lyotropic liquid crystalline lipid nanoparticles for the next generation of nanomedicine, *ACS Nano*, 2019, **13**(6), 6178–6206.

52 N. Tran, M. Hocquet, B. Eon, P. Sangwan, J. Ratcliffe, T. M. Hinton, J. White, B. Ozcelik, N. P. Reynolds and B. W. Muir, Non-lamellar lyotropic liquid crystalline nanoparticles enhance the antibacterial effects of rifampicin against Staphylococcus aureus, *J. Colloid Interface Sci.*, 2018, **519**, 107–118.

53 R. Negrini and R. Mezzenga, Diffusion, molecular separation, and drug delivery from lipid mesophases with tunable water channels, *Langmuir*, 2012, **28**(47), 16455–16462.

54 X. Mulet, B. J. Boyd and C. J. Drummond, Advances in drug delivery and medical imaging using colloidal lyotropic liquid crystalline dispersions, *J. Colloid Interface Sci.*, 2013, **393**, 1–20.

55 J. Clogston and M. Caffrey, Controlling release from the lipidic cubic phase. Amino acids, peptides, proteins and nucleic acids, *J. Controlled Release*, 2005, **107**(1), 97–111.

56 C. Caltagirone, M. Arca, A. M. Falchi, V. Lippolis, V. Meli, M. Monduzzi, T. Nylander, A. Rosa, J. Schmidt and Y. Talmon, Solvatochromic fluorescent BODIPY derivative as imaging agent in camptothecin loaded hexosomes for possible theranostic applications, *RSC Adv.*, 2015, **5**(30), 23443–23449.

57 B. Angelov, A. Angelova, S. K. Filippov, M. Drechsler, P. Štěpánek and S. Lesieur, Multicompartment Lipid Cubic Nanoparticles with High Protein Upload: Millisecond Dynamics of Formation, *ACS Nano*, 2014, **8**(5), 5216–5226.

58 F. Esmaeili, M. Hosseini-Nasr, M. Rad-Malekshahi, N. Samadi, F. Atyabi and R. Dinarvand, Preparation and antibacterial activity evaluation of rifampicin-loaded poly lactide-co-glycolide nanoparticles, *Nanomed. Nanotechnol. Biol. Med.*, 2007, **3**(2), 161–167.

59 N. Moghadas-Sharif, B. S. F. Bazzaz, B. Khameneh and B. Malaekeh-Nikouei, The effect of nanoliposomal formulations on Staphylococcus epidermidis biofilm, *Drug Dev. Ind. Pharm.*, 2015, **41**(3), 445–450.

60 B. S. F. Bazzaz, B. Khameneh, H. Zarei and S. Golmohammadzadeh, Antibacterial efficacy of rifampin loaded solid lipid nanoparticles against Staphylococcus epidermidis biofilm, *Microb. Pathog.*, 2016, **93**, 137–144.

61 T. Gebhardt, L. M. Wakim, L. Eidsmo, P. C. Reading, W. R. Heath and F. R. Carbone, Memory T cells in nonlymphoid tissue that provide enhanced local immunity during infection with herpes simplex virus, *Nat. Immunol.*, 2009, **10**(5), 524–530.

62 Y. Y. Chen, A. Angelova, B. Angelov, M. Drechsler, V. M. Garamus, R. Willumeit-Romer and A. H. Zou, Sterically stabilized spongosomes for multidrug delivery of anticancer nanomedicines, *J. Mater. Chem. B*, 2015, **3**(39), 7734–7744.

63 M. Valldeperas, M. Wisniewska, M. Ram-On, E. Kesselman, D. Danino, T. Nylander and J. Barauskas, Sponge Phases and Nanoparticle Dispersions in Aqueous Mixtures of Mono- and Diglycerides, *Langmuir*, 2016, **32**(34), 8650–8659.

64 C. Beaulac, S. Sachetelli and J. Lagace, In-vitro bactericidal efficacy of sub-MIC concentrations of liposome-encapsulated antibiotic against Gram-negative and Gram-positive bacteria, *J. Antimicrob. Chemother.*, 1998, **41**(1), 35–41.

65 D. Yang, D. Pornpattananangkul, T. Nakatsuji, M. Chan, D. Carson, C.-M. Huang and L. Zhang, The antimicrobial activity of liposomal lauric acids against Propionibacterium acnes, *Biomaterials*, 2009, **30**(30), 6035–6040.

66 B. P. Dyett, H. Yu, J. Strachan, C. J. Drummond and C. E. Conn, Fusion dynamics of cubosome nanocarriers with model cell membranes, *Nat. Commun.*, 2019, **10**(1), 1–13.

67 L. Boge, K. L. Browning, R. Nordström, M. Campana, L. S. Damgaard, J. Seth Caous, M. Hellsing, L. Ringstad and M. Andersson, Peptide-Loaded Cubosomes Functioning as an Antimicrobial Unit against Escherichia coli, *ACS Appl. Mater. Interfaces*, 2019, **11**(24), 21314–21322.

68 K. Floyd, P. Glaziou, A. Zumla and M. Raviglione, The global tuberculosis epidemic and progress in care, prevention, and research: an overview in year 3 of the End TB era, *Lancet Respir. Med.*, 2018, **6**(4), 299–314.

69 J. Davis, S. van Hal and S. Tong, in Combination antibiotic treatment of serious methicillin-resistant Staphylococcus aureus infections, *Seminars in respiratory and critical care medicine*, Thieme Medical Publishers, 2015, pp. 003–016.

70 G. E. Thwaitest, M. Scarborough, A. Szubert, P. S. Goncalves, M. Soares, J. Bostock, E. Nsutebu, R. Telly, R. Cunningham, J. Greig, S. A. Wyllie, P. Wilson, C. Auckland, J. Cairns, D. Ward, P. Lal, A. Guier, N. Jenkis, J. Sutton, M. Wiselka, G. R. Armando, C. Graham, P. R. Chadwick, G. Barlow, N. C. Goraon, B. Young, S. Meisner, P. McWhinney, D. A. Price, D. Harvey, D. Nayar, D. Jeyaratnam, T. Planche, J. Minton, F. Hudson, S. Hopkins, J. Williams, M. E. Torok, M. J. Llewelvo, J. D. Edgeworth, A. S. Walker and U. K. C. I. R. Grp, Adjunctive rifampicin to reduce early mortality from Staphylococcus aureus bacteraemia: the ARREST RCT, *Health Technol. Assess.*, 2018, **22**(59), 1–+.

71 W. Zimmerli and C. Moser, Pathogenesis and treatment concepts of orthopaedic biofilm infections, *FEMS Immunol. Med. Microbiol.*, 2012, **65**(2), 158–168.

72 D. Boraschi, P. Italiani, R. Palomba, P. Decuzzi, A. Duschl, B. Fadeel and S. M. Moghimi, Nanoparticles and innate immunity: new perspectives on host defence, *Semin. Immunol.*, 2017, **34**(C), 33–51.

73 L. Liu, Y. T. Liu, B. C. Xu, C. Y. Liu, Y. P. Jia, T. Liu, C. J. Fang, W. Wang, J. Ren, Z. Y. He, K. Men, X. Liang, M. Luo, B. Shao, Y. Mao, H. Y. Xiao, Z. Y. Qian, J. Geng, B. R. Dong, P. Mi, Y. Jiang, Y. Q. Wei and X. W. Wei, Negative regulation of cationic nanoparticle-induced inflammatory toxicity through the increased production of prostaglandin E2 *via* mitochondrial DNA-activated Ly6C(+) monocytes, *Theranostics*, 2018, **8**(11), 3138–3152.

74 S. Ryu, P. I. Song, C. H. Seo, H. Cheong and Y. Park, Colonization and Infection of the Skin by S. aureus: Immune System Evasion and the Response to Cationic Antimicrobial Peptides, *Int. J. Mol. Sci.*, 2014, **15**(5), 8753–8772.

75 G. Han, L. N. Nguyen, C. Macherla, Y. Chi, J. M. Friedman, J. D. Nosanchuk and L. R. Martinez, Nitric oxide–releasing nanoparticles accelerate wound healing by promoting fibroblast migration and collagen deposition, *Am. J. Pathol.*, 2012, **180**(4), 1465–1473.

76 K. Neibert, V. Gopishetty, A. Grigoryev, I. Tokarev, N. Al-Hajaj, J. Vorstenbosch, A. Philip, S. Minko and D. Maysinger, Wound-Healing with Mechanically Robust and Biodegradable Hydrogel Fibers Loaded with Silver Nanoparticles, *Adv. Healthcare Mater.*, 2012, **1**(5), 621–630.

77 R. Tada, H. Suzuki, S. Takahashi, Y. Negishi, H. Kiyono, J. Kunisawa and Y. Aramaki, Nasal vaccination with pneumococcal surface protein A in combination with cationic liposomes consisting of DOTAP and DC-chol confers antigen-mediated protective immunity against Streptococcus pneumoniae infections in mice, *Int. Immunopharmacol.*, 2018, **61**, 385–393.